(Received 11 October 2025, Accepted 28 November 2025, Scheduled 30 December 2025)

Synthesis of Planar Antenna Arrays Based on Subarray Division Using the ICOK-Hybrid Algorithm

Chenxin Ren*, Hua Guo, Yang Xiao, Peng Song, and Lijian Zhang

School of Electronics and Information, Xi'an Polytechnic University, Xi'an 710048, China

ABSTRACT: In modern wireless systems, such as radar, satellite communication, and 5G communication, planar antenna arrays can achieve high-performance radiation characteristics. The synthesis of these arrays that can produce patterns with low peak sidelobe levels (PSLL) is critical for improving the performance of the antenna system. However, the synthesis of large-scale planar arrays presents a complex nonlinear optimization challenge because of the vast number of variables which leads to high design complexity. To address these issues, an improved hybrid optimization method which is called ICOK-Hybrid Algorithm is proposed. The hybrid algorithm integrates Invasive Weed Optimization (IWO), Convex Optimization (CO), and K-means clustering. The convex optimization is used to efficiently optimize the excitation amplitudes and phases while the IWO algorithm is used to refine the positions of the array elements. Furthermore, an innovative subarray partitioning strategy based on an improved K-means algorithm was introduced to group elements with similar excitations which significantly reduces the design complexity and hardware costs. Numerical results demonstrate that the proposed algorithm achieves a significantly lower PSLL compared with the results obtained by other methods. The practical feasibility and reliability of the proposed approach are further verified by full-wave electromagnetic simulation software CST.

1. INTRODUCTION

Array antennas have been widely employed in radar and wireless communication systems [1]. Several important applications include beam forming [2], broadcasting [3], and radio-frequency identification (RFID) [4]. Array antennas usually have numerous optimization parameters. Therefore, the synthesis of antenna arrays becomes a high-dimensional optimization problem.

Compared with optimization algorithms such as Taylor synthesis method [5] and Chebyshev synthesis method [6], swarm intelligent optimization algorithms exhibit faster convergence, enhanced global convergence properties, and improved robustness. Therefore, these algorithms have been widely used in the synthesis of antenna arrays [7]. However, population-based intelligent optimization algorithms can fall into a local optimum, especially when addressing complex, non-convex or multimodal optimization problems [8]. To achieve a balance between global exploration and efficient convergence, many algorithms have integrated population-based intelligent optimization methods with convex optimization techniques. This type of hybrid optimization algorithm was initially proposed by Isernia et al. in 2004 [9]. In 2019, a novel method combining Cuckoo Optimization Algorithm (COA) with Convex Optimization (CO) was proposed to optimize the amplitude, phase and position of array elements while controlling the sidelobe level, beamwidth, and null placement [10]. The method in [11] is based on a combination of differential evolution (DE) optimization and convex optimization. During the optimization process, this hybrid strategy is also employed to optimize the element positions and excitations. Subarray division has been widely used to reduce the design complexity of antenna arrays. Subarray division is to divide a full array into several subarrays, and each subarray has the same excitation amplitude. This approach reduces the number of feed units and further lowers the design complexity and production cost of the array antenna [12]. In [13], a hybrid method integrating K-means clustering and Convex Optimization (CO) was proposed to design subarrays capable of producing multiple arbitrary functional beams. In [14], a weighted matrix was employed to improve K-means clustering, which fulfills the sidelobe suppression in rectangular uniform phased arrays.

Planar microstrip antennas have found widespread use in this field due to their low cost, broad bandwidth, and attractive profile [15]. In [16], a new band-notched printed monopole antenna with variable frequency band-notch characteristics is presented. The proposed antenna has a T-shaped parasitic element designed on the bottom of the substrate and a narrow circular slot etched on the patch to generate a high value VSWR notch band behavior. Ref. [17] presents an innovative and condensed blueprint for a UWB printed monopole antenna, aiming to augment bandwidth and achieve dual band-stop capabilities, all while accounting for the impact of the human body model on stop bands. In [18], a compact UWB monopole antenna with tunable multiband rejection is presented, with human-body effects incorporated to refine the stop-band response and improve bandwidth performance.

In this study, a novel hybrid optimization algorithm that integrates the Invasive Weed Optimization (IWO) algorithm, Convex Optimization (CO) techniques, and K-means clustering op-

* Corresponding author: Chenxin Ren (230411048@stu.xpu.edu.cn).

timization is proposed. Additionally, the IWO algorithm is employed to optimize the initial cluster centers of the K-means algorithm, which can improve the clustering performance. This approach achieves lower PSLL in the synthesis of planar array antenna patterns and significantly reduces the complexity and cost associated with the design of planar array antennas. Section 2 presents the optimization model. Section 3 details the optimization procedures of the proposed hybrid algorithm. Extensive numerical examples and comparative analyses are discussed in Section 4. In Section 5, full-wave simulations are conducted to demonstrate the reliability and effectiveness of the proposed hybrid optimization algorithm. Finally, Section 6 concludes this paper.

2. MATHEMATICAL MODEL

2.1. Mathematical Model of the Symmetrical Rectangular Array Antenna

The structure of a symmetrical rectangular sparse array antenna in the first quadrant is illustrated in Fig. 1. The array elements are located on the xoy plane and are symmetrically distributed with respect to both the x-axis and y-axis. The aperture size of the array is $2L \times 2H$, and the total number of elements is $4N$. The corresponding array factor is given by

$$AF(\theta,\phi) = \sum_{n=1}^{4N} w_n \exp\left(jkx_n \sin\theta\cos\phi + jky_n \sin\theta\sin\phi\right) \tag{1}$$

where w_n and (x_n, y_n) denote the excitation coefficient and the position of the nth array element, and $k = 2\pi/\lambda$ is the wave number, where λ is the operating wavelength; $\theta \in [0, \pi/2]$ and $\phi \in [0, 2\pi]$ represent the elevation angle and the azimuth angle, respectively. Due to the symmetry of the array element positions, Equation (1) can be rewritten by

$$\begin{aligned} AF(u,v) &= \sum_{n=1}^{4N} w_n \exp\left(jkx_n u + jky_n v\right) \\ &= 4\sum_{n=1}^{N} w_n \cos\left(kx_n u\right)\cos(ky_n v) \end{aligned} \tag{2}$$

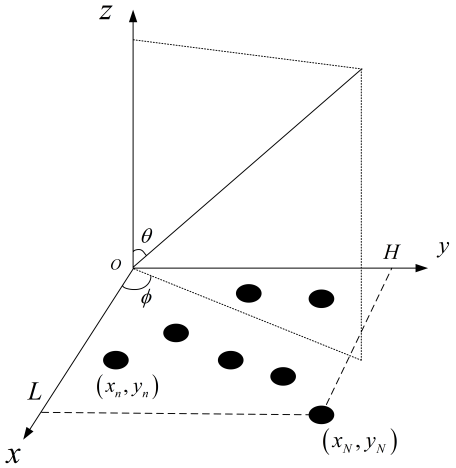

FIGURE 1. Symmetrical planar array antenna structure.

where $u = \sin\theta\cos\phi$, $v = \sin\theta\sin\phi$ are the angular coordinates. The peak sidelobe level of the radiation pattern can be given by

$$\mathrm{PSLL}\,(\mathrm{dB}) = \max\left\{20.0 \times \lg\left|\frac{AF(u,v)}{AF_{\max}}\right|_{(u,v)\in p_s}\right\} \tag{3}$$

where p_s denotes the sidelobe region, and $AF_{\max}$ is the maximum value of the main lobe level.

In this study, the optimization objective is to minimize the peak sidelobe level (PSLL) of the radiation pattern. A minimum spacing constraint of d_e is imposed between the adjacent array elements. Accordingly, the mathematical optimization model can be formulated as follows

$$\begin{cases} find.\,\mathbf{h} = (\mathbf{x},\mathbf{y},\mathbf{w}) \\ \min.\, f(\mathbf{h}) = PSLL \\ s.t.\,\sqrt{(x_m - x_n)^2 + (y_m - y_n)^2} \geq d_e \\ 1 \leq m,\, n \leq N,\, m \neq n \\ (x_N, y_N) = (L, H) \\ 0 \leq w_n \leq 1,\;\; n = 1, 2, ..., N \end{cases} \tag{4}$$

where the fitness $f(\mathbf{h})$ can be defined as the peak sidelobe level (PSLL), and $\mathbf{h} = (\mathbf{x},\mathbf{y},\mathbf{w})$ represents the optimal element positions and excitation coefficients that minimize the PSLL, where $\mathbf{x} = (x_1, ..., x_{N-1})^T$, $\mathbf{y} = (y_1, ..., y_{N-1})^T$ and $\mathbf{w} = [w_1, w_2, ..., w_n]^T$. The final constraint defines the allowable range for the normalized excitation weights assigned to each antenna element.

2.2. Mathematical Model of Convex Optimization

In Equation (2), variables $\mathbf{u}$ and $\mathbf{v}$ are sampled at G discrete points, where $\mathbf{u} = [u_1, \cdots, u_G]^T$, $\mathbf{v} = [v_1, \cdots, v_G]^T$. The array factor matrix $\mathbf{A}$ can be defined by

$$\mathbf{A} = \begin{bmatrix} \cos(kx_1u_1)\cos(ky_1v_1) & \cos(kx_2u_1)\cos(ky_2v_1) & \cdots & \cos(kx_Nu_1)\cos(ky_Nv_1) \\ \cos(kx_1u_2)\cos(ky_1v_2) & \cos(kx_2u_2)\cos(ky_2v_2) & \cdots & \cos(kx_Nu_2)\cos(ky_Nv_2) \\ \vdots & \vdots & \ddots & \vdots \\ \cos(kx_1u_G)\cos(ky_1v_G) & \cos(kx_2u_G)\cos(ky_2v_G) & \cdots & \cos(kx_Nu_G)\cos(ky_Nv_G) \end{bmatrix} \tag{5}$$

Let $\mathbf{w} = [w_1, w_2, ..., w_N]^T$, so $\mathbf{A}\cdot\mathbf{w}$ is the far-field power pattern of the antenna array.

For nonuniform planar antenna arrays, the mathematical model of the proposed CO algorithm is formulated as follows

$$\begin{cases} \min\limits_{w} \|\mathbf{A}(\mathbf{p}_s)\mathbf{w}\|_1 \\ s.t.\,\mathbf{A}(u_0,v_0)\mathbf{w} = 1 \\ |\mathbf{A}(\mathbf{p})\mathbf{w}| \leq 1 \\ |\mathbf{A}(\mathbf{p}_s)\mathbf{w}| \leq b \\ 0 \leq w_n \leq 1,\;\; n = 1, 2, ..., N \end{cases} \tag{6}$$

where (u_0, v_0) is the beam direction. $\mathbf{p}_s$ and $\mathbf{p}_m$ are the side lobe region and the main lobe region, respectively. b is the peak side lobe level.

2.3. Optimization of the Element Positions

To improve the global search capability of the algorithm and reduce its computational complexity, the position optimization problem of the two-dimensional planar array is transformed into an equivalent one-dimensional linear array optimization problem in this section. As illustrated in Fig. 2, the aperture to be optimized within the first quadrant of the symmetric planar array has a size of $L \times H$. It is assumed that all elements in this region are arranged along a series of lines parallel to the x-axis, with the vertical coordinates of the lines denoted as Y_m, where $m = 1, 2, \cdots, M$. The minimum element spacing constraint is denoted as d_e. To maintain the array structure, the positions of two elements are fixed as

$$\begin{cases} (x_1, y_1) = (l_0, h_0) \\ (x_N, y_N) = (L, H) \end{cases} \tag{7}$$

where $l_0 = h_0 = 0.5d_e$. If each row is uniformly arranged with the minimum allowable spacing, the total length occupied by the M rows is $(M-1)d_e$, and the remaining distance available for optimization along the y-axis is given by

$$SP_y = H - h_0 - (M-1)d_e = H - (M-0.5)d_e \tag{8}$$

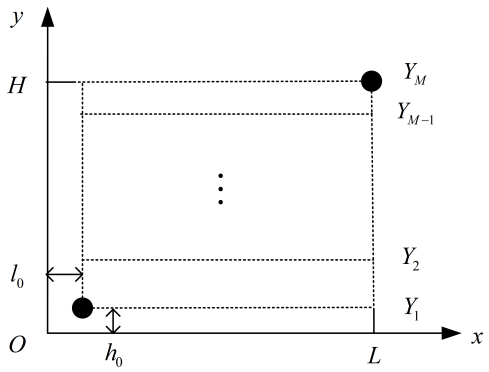

FIGURE 2. Schematic diagram of element position optimization.

Since the positions of Y_1 and Y_M are fixed, the number of rows that require optimization is $M-2$. A $(M-2)\times 1$ matrix $\mathbf{C}^y$ is generated, with each element being a random number uniformly distributed in the interval $[0, SP_y]$.

$$\mathbf{C}^y = \left[C_1^y, C_2^y, \cdots, C_{M-2}^y\right] \tag{9}$$

The elements of the matrix $\mathbf{C}^y$ are sorted in ascending order to form a new matrix $\mathbf{C}^{y'} = \left[C_1^{y'}, C_2^{y'}, \cdots, C_{M-2}^{y'}\right]$, where $C_1^{y'} \le C_2^{y'} \le \cdots \le C_{M-2}^{y'}$. Consequently, the y-coordinates of the array elements on each row can be determined as

$$Y_1 = h_0, \quad Y_M = H \tag{10a}$$

$$\begin{bmatrix} Y_2 \\ Y_3 \\ \cdots \\ Y_{M-1} \end{bmatrix} = Y_1 + \mathbf{C}^{y'} + \begin{bmatrix} d_e \\ 2d_e \\ \cdots \\ (M-1)d_e \end{bmatrix} = Y_1 + \begin{bmatrix} C_1^{y'} + d_e \\ C_2^{y'} + 2d_e \\ \cdots \\ C_{M-2}^{y'} + (M-2)d_e \end{bmatrix} \tag{10b}$$

Once the y-coordinates of the elements on each row are determined, the available element arrangement length for each row, denoted as l_m, and the total available arrangement length of the array, denoted as L_T, can be expressed as

$$\begin{cases} l_m = L - l_0 = L - 0.5d_e, \quad m = 1, 2, \cdots, M \\ L_T = \sum_{m=1}^{M} l_m \end{cases} \tag{11}$$

A new coordinate system is formed by connecting the ends of each line with a uniform spacing d_e between adjacent rows, as shown in Fig. 3. Its total length is

$$L_R = L_T + (M-1)d_e \tag{12}$$

In the newly defined coordinate system, the coordinates of each node can be expressed as:

$$\begin{cases} x_{L_1} = 0 \\ x_{L_m} = \sum_{i=1}^{m-1} l_i + (m-1)d_e, \quad m = 2, 3, \cdots, M \\ x_{H_m} = \sum_{i=1}^{m} l_i + (m-1)d_e, \quad m = 1, 2, \cdots, M \end{cases} \tag{13}$$

If N array elements are uniformly placed with the minimum distance d_e, the occupied length is $(N-1)d_e$. Accordingly, the remaining length that can be optimized is:

$$SP_x = L_R - (N-1)d_e \tag{14}$$

Similarly, since the positions of two elements are fixed, the remaining $(N-2)\times 1$ element positions must be optimized. A $(N-2)\times 1$ matrix $\mathbf{C}^x$ is generated, with its elements being random numbers uniformly distributed within the interval $[0, SP_x]$.

$$\mathbf{C}^x = \left[C_1^x, C_2^x, \cdots, C_{N-2}^x\right] \tag{15}$$

Similarly, the elements in the matrix $\mathbf{C}^x$ are sorted in ascending order to obtain a new matrix $\mathbf{C}^{x'} = \left[C_1^{x'}, C_2^{x'}, \cdots, C_{N-2}^{x'}\right]$, where $C_1^{x'} \le C_2^{x'} \le \cdots \le C_{N-2}^{x'}$. The corresponding positions of the array elements in the new coordinate system are thus determined by

$$xx_1 = 0, \quad xx_N = L_R \tag{16a}$$

$$\begin{bmatrix} xx_2 \\ xx_3 \\ \cdots \\ xx_{N-1} \end{bmatrix} = \mathbf{C}^{x'} + \begin{bmatrix} d_e \\ 2d_e \\ \cdots \\ (N-1)d_e \end{bmatrix} = \begin{bmatrix} C_1^{x'} + d_e \\ C_2^{x'} + 2d_e \\ \cdots \\ C_{N-2}^{x'} + (N-1)d_e \end{bmatrix} \tag{16b}$$

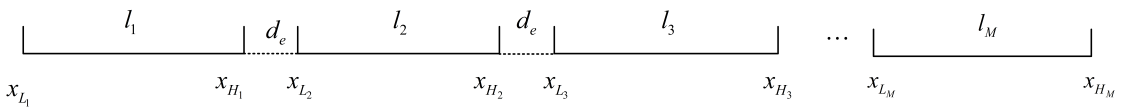

FIGURE 3. New one-dimensional coordinate system.

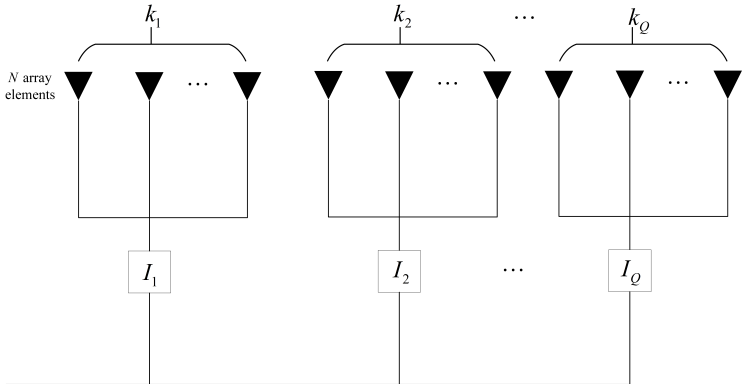

FIGURE 4. The structure of the subarray partition.

As shown in Fig. 3, to avoid the placement of array elements within the interval $xx_n \in (x_{H_m}, x_{L_{m+1}}), m = 1, 2, \cdots, M-1$, elements located in this region are repositioned. Let $d_l = x_{L_{m+1}} - xx_n$. The updated positions of these elements are accordingly determined as

$$xx_n = xx_n + d_l \tag{17}$$

To ensure a minimum spacing of d_e, if $xx_{n+1} - xx_n < d_e$, the position is corrected by setting $xx_{n+1} = xx_n + d_e$. The final element positions in the actual coordinate system are then given by

$$\begin{cases} x_n = 0.5d_e + xx_n - x_{L_m} \\ y_n = Y_m \\ n = 1, 2, \cdots, N, \ \ m = 1, 2, \cdots, M \end{cases} \tag{18}$$

2.4. Mathematical Model of Subarray Partition

To reduce the design cost and computational complexity of array antennas, subarray division techniques can be used to divide an entire antenna array into several subarrays. This approach effectively decreases the complexity of the array antenna systems [19].

In Fig. 4, the entire antenna array is divided into Q subarrays. In each subarray, the excitations of the elements are the same. The excitation coefficient of the qth subarray is I_q, $q = 1, 2, ..., Q$. Therefore, Eq. (2) can be written as

$$AF(u, v) = 4 \sum_{q=1}^{Q} I_q \sum_{n=1}^{N} \delta_{c_n,q} \cos(kx_n u) \cos(ky_n v) \tag{19}$$

where $c_n \in [1, Q]$ indicates that the nth element belongs to the qth subarray. $\delta_{c_n,q}$ denotes the Dirac delta function, which can be defined as follows

$$\delta_{c_n,q} = \begin{cases} 1, & c_n = q \\ 0, & \text{otherwise} \end{cases} \tag{20}$$

After the subarray division, the relationship between the excitation of the subarray and the excitation of each element can be expressed as

$$w_n = \sum_{q=1}^{Q} \delta_{c_n,q} I_q, \quad n = 1, 2, 3, \cdots, N \tag{21}$$

Therefore, the optimization model in Eq. (4) can be expressed as

$$\begin{cases} find. \mathbf{h} = (\mathbf{x}, \mathbf{y}, I_1, ..., I_Q) \\ \min. f(\mathbf{h}) = PSLL \\ s.t. \sqrt{(x_m - x_n)^2 + (y_m - y_n)^2} \geq d_e \\ 1 \leq m, n \leq N, \ m \neq n \\ (x_N, y_N) = (L, H) \\ 0 < I_q \leq 1, \ q = 1, 2, ..., Q \end{cases} \tag{22}$$

3. OPTIMIZATION ALGORITHM

3.1. Improved K-Means Clustering Optimization Algorithm

K-means clustering optimization algorithm is a widely used unsupervised learning algorithm that partitions data into Q clusters by minimizing the sum of squared distances between data points and their respective cluster centers. In Fig. 5(a), w_n, $n = 1, 2, ..., N$, are the original element excitation coefficients. I_q, $q = 1, 2, ..., Q$, represents the cluster centers which are also the excitation coefficients of each subarray. Fig. 5(b)

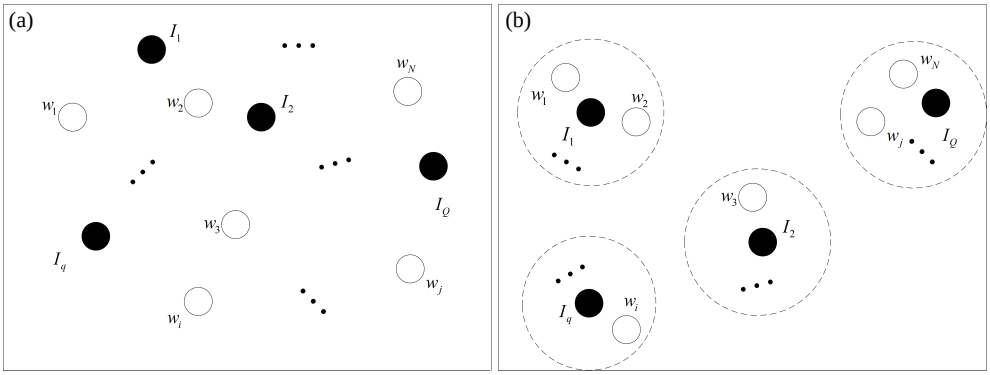

FIGURE 5. (a) Original array element excitation distribution in a rectangular array antenna. (b) Optimized element excitation distribution.

presents the excitation distribution after subarray partitioning. In Fig. 5(b), each element excitation is assigned to the subarray excitation by grouping the element excitations that are closest to the initial cluster centers through the K-means clustering algorithm.

If the initial cluster centers in the K-means clustering algorithm are selected randomly, the optimization performance can be affected. To overcome this limitation, the cluster centers are treated as optimization parameters and are updated through the process of IWO. Since the fitness function is designed to minimize the PSLL, the optimization of the cluster centers can make the PSLL much lower. The steps of the K-means clustering optimization algorithm are as follows.

Step 1: Let the iteration number of the K-means optimization algorithm $iteration = 0$ and the maximum value of the iteration number be denoted by $iteration\_\max = 20$. Give the initial clustering center $I_q^{(0)}$, $q = 1, 2, ..., Q$ by the method introduced above.

Step 2: Calculate the distance between each data element and all cluster centers in sequence, and assign it to the nearest center. Specifically, compute the distance $d_{nq} = \sqrt{\left|w_n - I_q^{(iteration)}\right|^2}$ between the element excitation amplitude w_n and the subarray excitation amplitude $I_q^{(iteration)}$.

Step 3: If d_{nq} is the minimum value in the vector $d = [d_{1q}, d_{1q}, \cdots, d_{Nq}]^T$, then $c_n = q$, indicating that the nth array element belongs to the qth subarray. The total number of elements in the first q subarrays is N_q. Prior to contiguous subarray division, the excitation coefficients must be sorted in descending order before proceeding with the division process. And $I_q^{(iteration+1)}$ can be expressed as

$$I_q^{(iteration+1)} = \frac{\sum_{n=1}^{N} w_n \delta_{c_n,q}}{k_q} \tag{23}$$

where k_q denotes the element number of the qth subarray, which is illustrated in Fig. 4.

Step 4: Let $iteration = iteration + 1$. If $iteration < iteration\_\max$, return to Step 2. Otherwise, the output excitation coefficients I_q, $q = 1, 2, ..., Q$.

3.2. Optimization Steps of the ICOK-Hybrid Algorithm

The optimization procedure of the ICOK-Hybrid Algorithm for the rectangular array antenna is described as follows.

Step 1: A random $P \times R$ dimensional matrix **s** is generated as the initial population. So the initial matrix **s** can be expressed as:

$$\mathbf{s} = \begin{bmatrix} s_1^1 & s_2^1 & \cdots & s_R^1 \\ s_1^2 & s_2^2 & \cdots & s_R^2 \\ \cdots & \cdots & \cdots & \cdots \\ s_1^P & s_2^P & \cdots & s_R^P \end{bmatrix} \tag{24}$$

where P is the initial population size of the IWO algorithm, and $R = N + M + Q - 5$ is the dimension of the optimization parameters.

The matrix **s** can also be expressed as $\mathbf{s} = \left[s^1, s^2, ..., s^P\right]^T$. In every s^p, $p = 1, 2, ..., P$, the first $N + M - 4$ elements are used to optimize the element positions. The last $Q - 1$ elements are used to optimize the initial cluster centers.

Step 2: Define the array configuration, including the total number of elements $4N$, the aperture of each element $2H \times 2L$, the number of subarrays $4Q$. Give the parameters of the Invasive Weed Optimization (IWO) algorithm and let $iter = 1$.

Step 3: Taking the first $N + M - 4$ elements of s^p as optimization parameters, the element positions of the array antenna are updated using Eq. (18).

Step 4: The optimized positions are put into the CO model as formulated in Eq. (6) to calculate the element excitations of the antenna array.

Step 5: Taking the last $Q - 1$ elements of s^p as the initial cluster centers, the excitation amplitude of each subarray can be calculated by the optimization procedure introduced in Section 3.1.

Step 6: The optimized excitations of each subarray and the element positions of the antenna arrays are put into Eq. (22) to calculate the fitness value. The optimization parameters that can produce the lowest PSLL are saved as the ultimate results.

Step 7: The optimization parameters are optimized by IWO.

Step 8: Let $iter = iter + 1$, if $iter < iter_{\max}$, return Step 3. Otherwise, terminate the iteration and output the best result.

The flowchart of the hybrid algorithm is shown in Fig. 6.

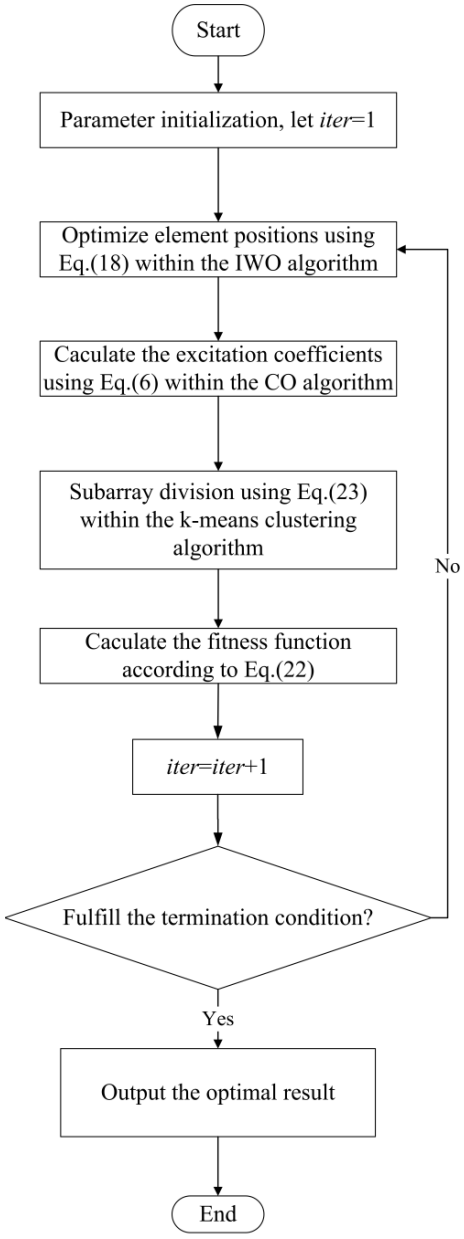

FIGURE 6. Optimization process of the hybrid optimization algorithm.

4. NUMERICAL RESULT

To validate the reliability and effectiveness of the proposed hybrid optimization algorithm, three examples of nonuniform symmetric rectangular arrays with varying numbers of elements are presented. Each calculation runs 20 times independently. The best, worst, and average results are preserved. Detailed IWO parameters are provided in Table 1. All computations were performed in MATLAB R2023b on a system with 16 GB RAM and an Intel Core i7-9750H processor.

TABLE 1. The parameters of IWO.

P	$P_{\max}$	σ_{ini}	σ_{fin}	$seed_{\max}$	$seed_{\min}$	n_{seed}
10	30	0.1	0.0001	12	1	3

In Table 1, P is the initial population size while $P_{\max}$ represents the maximum population size. σ_{ini} and σ_{fin} are the initial and final standard deviations, respectively. $seed_{\max}$ and $seed_{\min}$ are the maximum and minimum numbers of seeds that can be produced by a single weed. n_{seed} is the nonlinear modulation factor.

4.1. Example 1: Synthesis of Planar Array Antenna with 100-Element

In the first example, a rectangular plane array with $4N = 100$ array elements is synthesized. The aperture size is $2L \times 2H = 9.5\lambda \times 4.5\lambda$. And the minimum element spacing d_e is set to be 0.5λ. The beam direction is $(u_0, v_0) = (0°, 0°)$ and the side lobe region is $p_s \in [0.34, 1]$. The number of element rows after position optimization is set to $M = 4$. To ensure a fair comparison, the iteration of the IWO algorithm is set to $iter_{\max} = 300$.

As shown in Fig. 7, the radiation pattern corresponding to the best result obtained from 20 independent runs with $Q = 5$ subarrays is given. Fig. 8 presents the iteration curves of the PSLL obtained by the three optimization algorithms. The proposed method achieves a final PSLL of -31.57 dB while the PSO and DE algorithms converge to -26.60 dB and -25.05 dB, respectively. Fig. 9 provides a depiction of the spatial distribution of array elements along with their excitation magnitudes. Fig. 10 presents the optimized element position distributions. Since the study focuses on optimizing a symmetric rectangular planar array, only the element distribution in the first quadrant is displayed. Table 2 summarizes the runtime and the optimal results obtained by the three algorithms when the number of array elements is $2N = 100$ and the number of subarrays is $Q = 5$. As shown in Table 2, the IWO algorithm requires less time per iteration and simultaneously achieves a lower PSLL. Tables 3 and 4 list the detailed optimized positions and the corresponding excitation amplitudes, respectively.

TABLE 2. Computational efficiency of different algorithms for a $4N = 100$ element array ($Q = 5$).

Algorithm	Best Value (dB)	Runtime (s)
Proposed	-31.57	80.95
DE	-25.05	84.05
PSO	-26.60	83.61

Table 5 presents a comparison between the proposed hybrid optimization algorithm and results reported in related literature. When the number of subarrays is set to $Q = 5$, the proposed method achieves a peak sidelobe level (PSLL) of -31.57 dB. When $Q = 3$, the PSLL is -28.85 dB. In 20 independent optimization runs, the variance of the PSLL optimization results is 0.2882 when $Q = 5$, whereas the variance increases to 0.4481 when $Q = 3$. Compared with existing methods, the proposed algorithm demonstrates a notable advantage in suppressing PSLL.

In the synthesis of the antenna array using the proposed method, the parameter $P_{\max}$ in the IWO algorithm has a great influence on the optimization performance. To assess this ef-

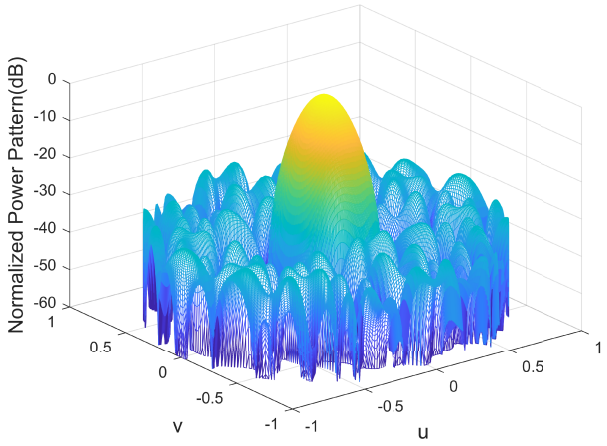

FIGURE 7. The far-field power pattern of the 100-element array ($Q = 5$).

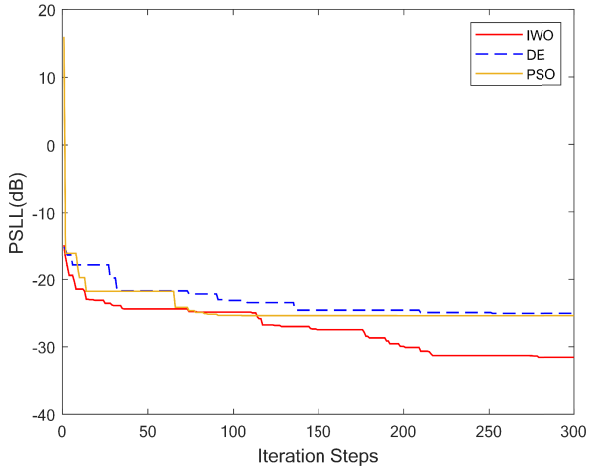

FIGURE 8. Iterative convergence curve for the 100-element array ($Q = 5$).

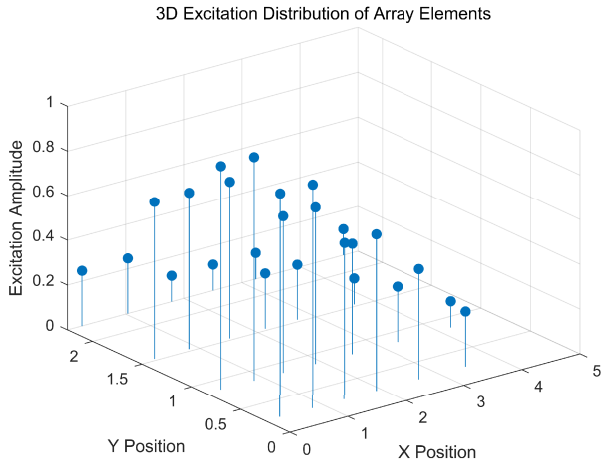

FIGURE 9. Excitation amplitude distribution of 100 elements ($Q = 5$) in the first quadrant.

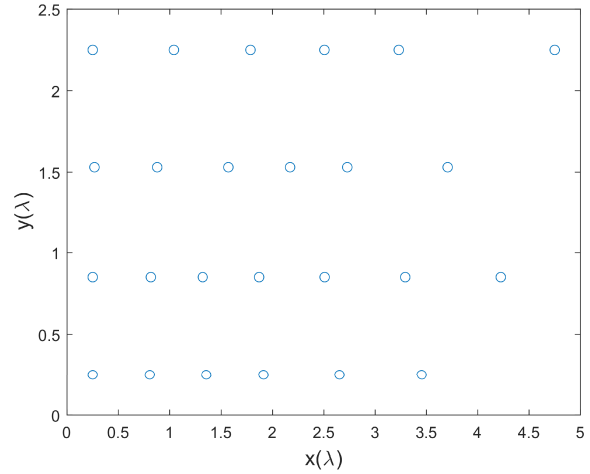

FIGURE 10. Spatial distribution of 100 array elements ($Q = 5$) in the first quadrant.

TABLE 3. Optimized element positions of the 100 array elements ($Q = 5$).

Number	(x, y)	Number	(x, y)	Number	(x, y)	Number	(x, y)	Number	(x, y)
1	0.25, 0.25	6	3.456, 0.25	11	2.517, 0.85	16	1.561, 1.529	21	1.037, 2.25
2	0.812, 0.25	7	0.25, 0.85	12	3.3, 0.85	17	2.172, 1.529	22	1.793, 2.25
3	1.36, 0.25	8	0.822, 0.85	13	4.224, 0.85	18	2.726, 1.529	23	2.502, 2.25
4	1.909, 0.25	9	1.324, 0.85	14	0.266, 1.529	19	3.707, 1.529	24	3.238, 2.25
5	2.65, 0.25	10	1.882, 0.85	15	0.864, 1.529	20	0.25, 2.25	25	4.75, 2.25

fect, the algorithm runs 20 times when the antenna array has $4N = 100$ array elements and $Q = 5$ subarrays. The results are summarized in Table 6. As shown in Table 6, if $P_{\max}$ increases from 20 to 30, the best PSLL has an improvement of more than 1 dB. However, when $P_{\max}$ increases from 30 to 40, the best PSLL has an improvement of less than 0.2 dB. Considering both optimization effectiveness and computational efficiency, $P_{\max}$ is set to be 30 in this study.

4.2. Example 2: Synthesis of Planar Array Antenna with 264-Element

In the second example, the number of array elements is $4N = 264$. Its main lobe width is 20°. So, the CO model, which is introduced in Eq. (6), is used where $(u_0, v_0) = (0°, 0°)$, $p_s \in [0.34, 1]$. The minimum array element spacing is set to be 0.5λ. The antenna array is configured with $Q = 7$ and $Q = 5$ subarrays. The number of element rows after position optimization is set to $M = 11$. The aperture of this planar array antenna

TABLE 4. Optimized excitation coefficients of the 100 array elements ($Q = 5$).

Number	Exact numerical values of the excitation coefficients				
1∼5	1.0000	1.0000	0.6996	0.6996	0.4926
6∼10	0.2462	1.0000	1.0000	0.6996	0.6996
11∼15	0.4926	0.2462	0.1158	0.6996	0.6996
16∼20	0.6996	0.2462	0.2462	0.1158	0.2462
21∼25	0.2462	0.1158	0.1158	0.1158	0.1158

TABLE 5. Comparison with other literature.

Methods	PSLL (dB)	Gain (dBi)
Proposed method ($Q = 5$)	-31.57	33.66
Proposed method ($Q = 3$)	-28.85	33.06
The method in [20]	-18.840	-
The method in [21]	-20.384	-
The method in [22]	-21.886	-
The method in [23]	-22.195	-

TABLE 6. The influence of $P_{\max}$ on the synthesis results.

$P_{\max}$	The best result (dB)	The average result (dB)	The worst result (dB)
20	-30.24	-30.14	-29.02
30	-31.57	-31.03	-30.07
40	-31.63	-31.12	-30.07

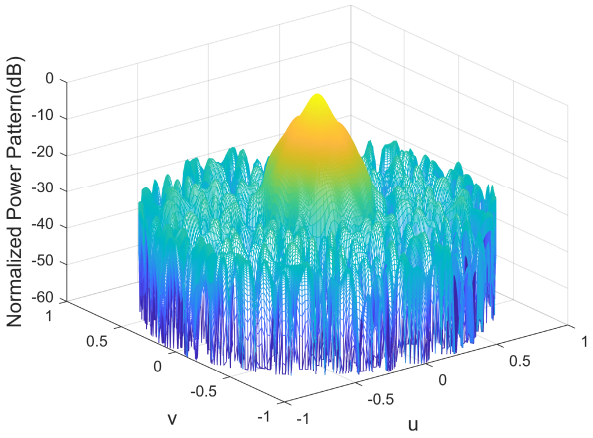

FIGURE 11. The far-field power pattern of the 264-element array ($Q = 7$).

is $2L \times 2H = 16\lambda \times 13\lambda$ and the max iteration $iter_{\max}$ is set to be 300.

Figure 11 shows the radiation pattern corresponding to the best result among 20 independent runs with $Q = 7$. In 20 independent optimization runs, the variance of the PSLL optimization results is 0.2547 when $Q = 7$, whereas it increases to 0.3256 when $Q = 5$. Fig. 12 illustrates the iteration trajectories for the 264-element array antenna under the three optimization algorithms. The IWO method achieves a final PSLL

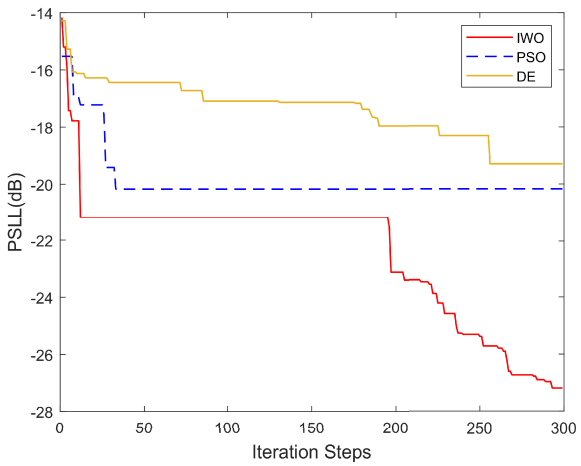

FIGURE 12. Iterative convergence curve for the 264-element array ($Q = 7$).

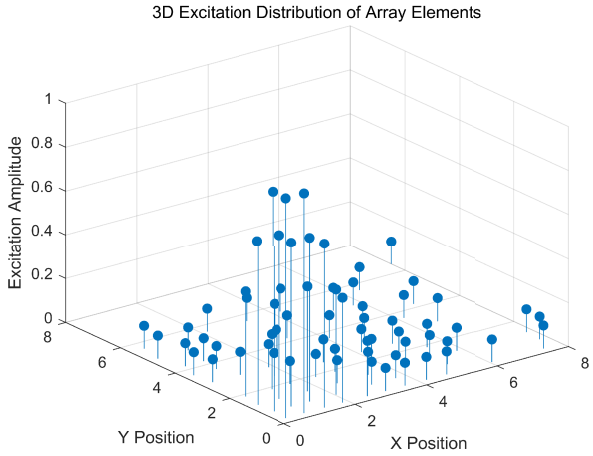

FIGURE 13. Excitation amplitude distribution of 264 elements ($Q = 7$) in the first quadrant.

TABLE 7. Computational efficiency of different algorithms for a $4N = 264$ element array ($Q = 7$).

Algorithm	Best Value (dB)	Runtime (s)
Proposed	-27.19	285.89
DE	-19.29	305.14
PSO	-20.17	303.32

of -27.19 dB, while the PSO and DE approaches converge to -20.17 dB and -19.29 dB, respectively. Fig. 13 and Fig. 14 present the optimized excitation amplitudes and the spatial distribution of the array elements, respectively. Table 7 presents a comparison of the optimal results and the average runtime per iteration of the three algorithms when the number of array elements is $4N = 264$ and the number of subarrays is $Q = 7$. As shown in Table 7, the proposed ICOK hybrid optimization algorithm not only demonstrates superior optimization capability but also achieves a lower computational cost per iteration. The detailed numerical results of the optimized element positions and excitations obtained using the hybrid optimization al-

TABLE 8. Optimized element positions of the 264 array elements ($Q = 7$).

Element number	(x, y)	Element number	(x, y)	Element number	(x, y)	Element number	(x, y)	Element number	(x, y)
1	0.25, 0.25	15	2.044, 0.75	29	0.358, 1.889	43	1.879, 3.032	57	1.098, 4.955
2	0.763, 0.25	16	3.041, 0.75	30	1.098, 1.889	44	4.581, 3.032	58	3.53, 4.955
3	1.332, 0.25	17	3.713, 0.75	31	1.627, 1.889	45	6.634, 3.032	59	5.192, 4.955
4	1.84, 0.25	18	5.154, 0.75	32	2.351, 1.889	46	0.25, 3.641	60	5.751, 4.955
5	2.537, 0.25	19	7.766, 0.75	33	2.885, 1.889	47	0.886, 3.641	61	0.383, 5.633
6	3.044, 0.25	20	0.25, 1.292	34	3.907, 1.889	48	2.58, 3.641	62	2.155, 5.633
7	3.586, 0.25	21	0.862, 1.292	35	4.672, 1.889	49	4.075, 3.641	63	3.263, 5.633
8	4.186, 0.25	22	1.658, 1.292	36	5.463, 1.889	50	5.005, 3.641	64	4.227, 5.633
9	4.753, 0.25	23	2.488, 1.292	37	1.64, 2.515	51	6.157, 3.641	65	6.445, 5.633
10	6.044, 0.25	24	3.354, 1.292	38	3.044, 2.515	52	0.445, 4.205	66	8,6.5
11	7.49, 0.25	25	4.402, 1.292	39	4.104, 2.515	53	0.959, 4.205		
12	0.284, 0.75	26	5.078, 1.292	40	4.972, 2.515	54	3.321, 4.205		
13	0.787, 0.75	27	5.836, 1.292	41	0.314, 3.032	55	6.862, 4.205		
14	1.302, 0.75	28	7.812, 1.292	42	1.086, 3.032	56	0.25, 4.955		

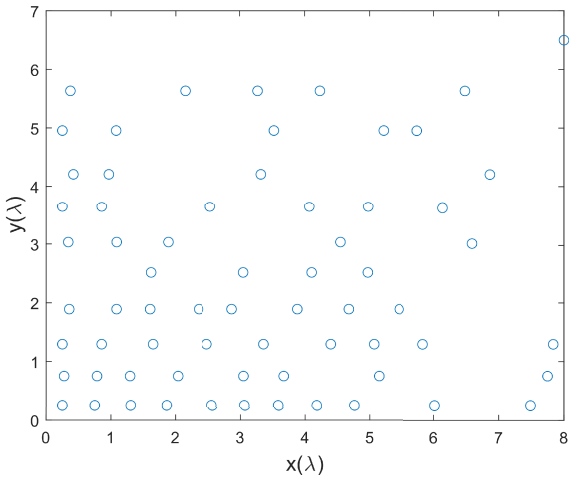

FIGURE 14. Spatial distribution of 264 array elements ($Q = 7$) in the first quadrant.

gorithm are listed in Tables 8 and 9. In Table 10, the proposed hybrid algorithm achieves the best PSLL of -27.19 dB when the number of subarrays is $Q = 7$, and -26.60 dB when $Q = 5$, demonstrating a clear advantage over the method reported in Ref. [24].

5. FULL-WAVE SIMULATION

To validate the reliability of the proposed hybrid optimization algorithm, a full-wave simulation experiment is carried out using CST Microwave Studio software. This section presents a full-wave simulation validation of the subarray configuration with $Q = 5$ obtained in Example 1. The positions and excitation amplitudes of the array elements are provided in Table 3 and 4, respectively.

In this experiment, the center frequency of the antenna is set to 30 GHz. The antenna elements adopt a rectangular microstrip patch configuration, as illustrated in Fig. 15. The width w_p of each patch is 3.6 mm and the length L_p is 2.6 mm. A slit with a depth of 0.7 mm (L_s) and a width of 1.5 mm (w_s) is etched on the patch to achieve proper impedance matching. The thickness of the metallic layer of the patch is 0.018 mm. The antenna elements are printed on a Rogers 4350B substrate with a thickness of 0.254 mm (relative dielectric constant of 3.48,

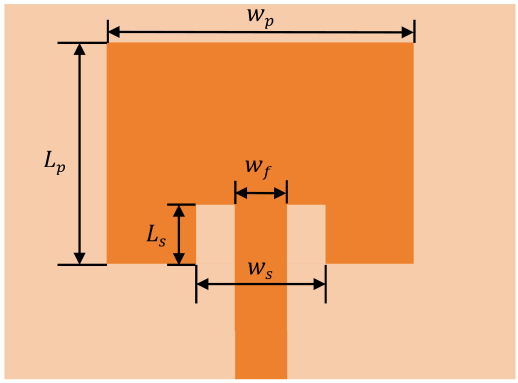

FIGURE 15. Microstrip patch antenna.

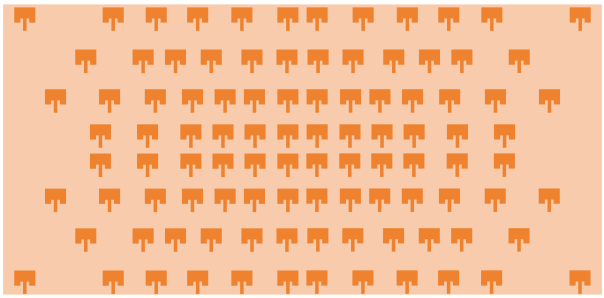

FIGURE 16. Full-wave simulation model of a 100-element array.

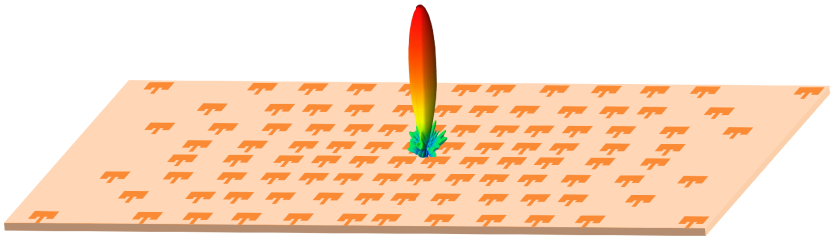

FIGURE 17. 3D full-wave electromagnetic simulation of the rectangular array antenna.

TABLE 9. Optimized excitation coefficients of the 264 array elements ($Q = 7$).

Element number	Precise excitation coefficients of the array elements					
1∼6	1.0000	1.0000	0.7447	0.4753	0.2494	0.1039
7∼12	0.1039	0.1039	0.1039	0.1039	0.1039	1.0000
13∼18	0.7447	0.7447	0.4753	0.1039	0.1039	0.1039
19∼24	0.1039	0.7447	0.7447	0.4753	0.1039	0.1039
25∼30	0.1039	0.1039	0.1039	0.1039	0.4753	0.2494
31∼36	0.1039	0.1039	0.1039	0.1039	0.1039	0.1039
37∼42	0.1039	0.1039	0.1039	0.1039	0.1039	0.1039
43∼48	0.1039	0.1039	0.1039	0.1039	0.1039	0.1039
49∼54	0.1039	0.1039	0.1039	0.1039	0.1039	0.1039
55∼60	0.1039	0.1039	0.1039	0.1039	0.1039	0.1039
61∼66	0.1039	0.1039	0.1039	0.1039	0.1039	0.1039

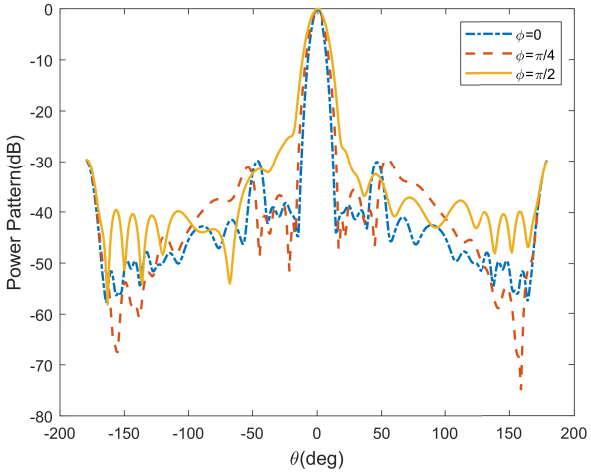

FIGURE 18. Full-wave electromagnetic simulation of a 100-element antenna array.

loss tangent of 0.0037). In addition, Fig. 16 presents the 100-element array antenna model designed based on the proposed hybrid optimization approach.

Figure 17 illustrates the 3D radiation pattern of the full array composed of the proposed rectangular microstrip patch antennas. Fig. 18 shows the radiation patterns of the simulated array in three different directions, obtained from the CST full-wave simulation. In particular, the full-wave simulation results show that the proposed array model achieves a PSLL of -29.6 dB at $\phi = 0°$, -30.7 dB at $\phi = 45°$, and -29.6 dB at $\phi = 90°$, respectively.

TABLE 10. Comparison of relevant literature.

Method	PSLL (dB)	Gain (dBi)
Proposed method ($Q = 7$)	-27.19	31.82
Proposed method ($Q = 5$)	-26.60	31.78
The method in [24]	under -20	-

6. CONCLUSION

In this study, the ICOK-Hybrid algorithm that combines the Invasive Weed Optimization (IWO) algorithm, convex optimization, and the K-means clustering algorithm is employed to optimize rectangular planar antenna arrays. The primary objective is to reduce the peak sidelobe level (PSLL) by jointly optimizing the element excitations and positions. To further reduce the design complexity and cost of planar arrays, a subarray partitioning strategy is also incorporated. The proposed hybrid algorithm enables simultaneous optimization of subarray excitations, element positions, and the total number of elements. This study investigates array optimization under varying aperture sizes and the number of elements. Also, subarray division is applied. Compared with existing methods in the literature, the proposed hybrid optimization algorithm achieves significantly lower PSLL, which demonstrates its effectiveness and superiority. Furthermore, full-wave electromagnetic simulation experiments were performed to verify the reliability of the proposed hybrid optimization algorithm.

ACKNOWLEDGEMENT

This work was supported by the Natural Science Basic Research Program of Shaanxi under Grant [number 2023-JC-YB-548], the Natural Science Basic Research Program of Shaanxi under Grant [number 2024JC-YBQN-0312] and Natural Science Foundation Program under Grant [number 2025JC-YBMS-254] of Shaanxi Provincial Science Technology Department.

REFERENCES

[1] Balanis, C. A., *Antenna Theory: Analysis and Design*, John Wiley & Sons, Hoboken, 2016.

[2] Godara, L. C., "Application of antenna arrays to mobile communications. II. Beam-forming and direction-of-arrival considerations," *Proceedings of the IEEE*, Vol. 85, No. 8, 1195–1245, 1997.

[3] Godara, L. C., "Applications of antenna arrays to mobile communications. I. Performance improvement, feasibility, and system considerations," *Proceedings of the IEEE*, Vol. 85, No. 7, 1031–1060, 1997.

[4] Abbak, M. and I. Tekin, "RFID coverage extension using microstrip-patch antenna array [wireless corner]," *IEEE Antennas and Propagation Magazine*, Vol. 51, No. 1, 185–191, 2009.

[5] Oh, K. J., H. Y. Lee, S. J. Kim, Y. S. Chung, and C. Cheon, "A study on wideband adaptive beamforming using Taylor weighting and LSMI algorithm," *Transactions of the Korean Institute of Electrical Engineers*, Vol. 62, No. 3, 380–386, 2013.

[6] Saputra, Y. P., F. Oktafiani, Y. Wahyu, and A. Munir, "Side lobe suppression for X-band array antenna using Dolph-Chebyshev power distribution," in *2016 22nd Asia-Pacific Conference on Communications (APCC)*, 86–89, Yogyakarta, Indonesia, 2016.

[7] Shen, G., Y. Liu, G. Sun, T. Zheng, X. Zhou, and A. Wang, "Suppressing sidelobe level of the planar antenna array in wireless power transmission," *IEEE Access*, Vol. 7, 6958–6970, 2019.

[8] Pandey, H. M., A. Chaudhary, and D. Mehrotra, "A comparative review of approaches to prevent premature convergence in GA," *Applied Soft Computing*, Vol. 24, 1047–1077, 2014.

[9] Isernia, T., F. J. A. Pena, O. M. Bucci, M. D'Urso, J. F. Gomez, and J. A. Rodriguez, "A hybrid approach for the optimal synthesis of pencil beams through array antennas," *IEEE Transactions on Antennas and Propagation*, Vol. 52, No. 11, 2912–2918, 2004.

[10] Khodier, M., "Comprehensive study of linear antenna array optimisation using the cuckoo search algorithm," *IET Microwaves, Antennas & Propagation*, Vol. 13, No. 9, 1325–1333, 2019.

[11] Fang, S., W. Li, Z. Xue, and W. Ren, "Synthesis of distributed array consisting of two subarrays via hybrid method of differential evolution optimization and convex optimization," *IEEE Antennas and Wireless Propagation Letters*, Vol. 20, No. 2, 125–129, 2021.

[12] Kerby, K. C. and J. T. Bernhard, "Sidelobe level and wideband behavior of arrays of random subarrays," *IEEE Transactions on Antennas and Propagation*, Vol. 54, No. 8, 2253–2262, 2006.

[13] Gong, Y., S. Xiao, Y. Zheng, and B. Wang, "An effective hybrid synthesis strategy of multibeam subarray," *IEEE Transactions on Antennas and Propagation*, Vol. 70, No. 4, 2623–2632, 2022.

[14] Zhao, J., J. Huang, Y. Cui, N. Zhang, Y. Wang, and Z. Wang, "Subarray partition based on sparse array weighted K-means clustering," *Electronics Letters*, Vol. 60, No. 18, e70042, 2024.

[15] Ojaroudi, M., C. Ghobadi, and J. Nourinia, "Small square monopole antenna with inverted T-shaped notch in the ground plane for UWB application," *IEEE Antennas and Wireless Propagation Letters*, Vol. 8, 728–731, 2009.

[16] Abdollahvand, M., H. R. Hassani, and G. R. Dadashzadeh, "Novel modified monopole antenna with band-notch characteristic for UWB application," *IEICE Electronics Express*, Vol. 7, No. 16, 1207–1213, 2010.

[17] Abdollahvand, M., Y. Zehforoosh, B. Marufi, P. E. Kaleybar, and A. Dastranj, "A novel UWB in-body printed microstrip feed monopole antenna with dual band-stop capabilities," *Microwave and Optical Technology Letters*, Vol. 66, No. 9, e34317, 2024.

[18] Abdollahvand, M., M. Khorshidi, S. Sobhi-Givi, and S. Ghosh, "An innovative in-body adjustable triple-band notch UWB monopole antenna with improved bandwidth performance," *Scientific Reports*, Vol. 15, No. 1, 24538, 2025.

[19] Yang, X., W. Xi, Y. Sun, T. Zeng, T. Long, and T. K. Sarkar, "Optimization of subarray partition for large planar phased array radar based on weighted K-means clustering method," *IEEE Journal of Selected Topics in Signal Processing*, Vol. 9, No. 8, 1460–1468, 2015.

[20] Chen, K., X. Yun, Z. He, and C. Han, "Synthesis of sparse planar arrays using modified real genetic algorithm," *IEEE Transactions on Antennas and Propagation*, Vol. 55, No. 4, 1067–1073, 2007.

[21] Liu, H., H. Zhao, W. Li, and B. Liu, "Synthesis of sparse planar arrays using matrix mapping and differential evolution," *IEEE Antennas and Wireless Propagation Letters*, Vol. 15, 1905–1908, 2016.

[22] Dai, D., M. Yao, H. Ma, W. Jin, and F. Zhang, "An asymmetric mapping method for the synthesis of sparse planar arrays," *IEEE Antennas and Wireless Propagation Letters*, Vol. 17, No. 1, 70–73, 2018.

[23] Tian, X., B. Wang, K. Tao, and K. Li, "An improved synthesis of sparse planar arrays using density-weighted method and chaos sparrow search algorithm," *IEEE Transactions on Antennas and Propagation*, Vol. 71, No. 5, 4339–4349, 2023.

[24] Yang, J., F. Yang, P. Yang, and Z. Xing, "A hybrid approach for the synthesis of planar thinned arrays with sidelobes reduction," in *2020 IEEE International Symposium on Antennas and Propagation and North American Radio Science Meeting*, 269–270, Montreal, QC, Canada, 2020.